Nickel-titanium pseudo-elastic behavior under equi-biaxial dynamic loading conditions

Pierre Quillery, Bastien Durand, Olivier Hubert, Han Zhao

Nickel-titanium pseudo-elastic behavior under equi-biaxial dynamic loading conditions

Pierre Quillery[1,⋆], *Bastien* Durand[1,⋆⋆], *Olivier* Hubert[1,⋆⋆⋆], and *Han* Zhao[12,⋆⋆⋆⋆]

[1] *LMT, ENS Paris-Saclay / Université Paris-Saclay / CNRS, 61 avenue du Président Wilson 94230 Cachan, France*
[2] *UFR Ingénierie, Université Pierre et Marie Curie, Sorbonne Universités, Paris*

Abstract. Shape memory alloys (SMA) undergo a solid-solid phase transformation called martensitic transformation, involving a "high temperature" phase, austenite and a "low temperature" phase, martensite. This transformation can be activated by thermal loading (heating or cooling) or mechanical loading (stress) and explains for example the pseudo-elastic phenomenon where high reversible deformation (>6%) can be reached during a tensile loading. Although the uniaxial dynamic pseudoelastic behavior of SMA is relatively well documented today, this behavior under multiaxial stress remains unknown. Such knowledge is however essential for the validation of multiaxial models to democratize the use of these materials. The stress-strain pseudo-elastic behavior of a Nickel-Titanium under equi-biaxial dynamic compression is addressed in this work. It is measured thanks to a new homemade equi-biaxial impact testing set-up using split Hopkinson bar. The use of thermal and optical camera allows strain and heating sources fields to be identified. The stress field is estimated by combining the strain gauges information placed on a coaxial transmitted bar and a transmitted tube and a finite element analysis of the specimen. The deformation appears homogeneous in the biaxial loading region of interest where a significant rise in temperature due to the phase change latent heat is observed. The dynamic testing allows on the other hand an equivalent dynamic stress/strain curve under biaxial and quasi-adiabatic conditions to be plotted. Experiments are finally compared to the results of finite difference axisymmetric model where the constitutive law is given by a fully coupled stochastic multiscale model.

1 Introduction

The solid-solid phase transformation can be activated in SMA by a thermal loading (heating or cooling) or a mechanical loading (stress) and explains for example the pseudo-elastic phenomenon where high reversible deformations (>6%) can be reached during a tensile loading. Although the uni-axial dynamic pseudo elastic behavior of SMA is relatively well documented today, behavior under multiaxial stress remains unknown. Such knowledge is however essential for the validation of multi-axial models, and finally for the democratization of these materials in current applications. SMA are subject to complex stress states, due to thermal and mechanical loadings and due to their geometries. For super-elasticity as well as shape memory effect, the nickel-titanium behavior is non-linear and stress states are multi-axial. The description of first order austenite to martensite phase transformation is usually enough to model uni-axial behaviors [1]. A multiscale description of the material under multi-axial loadings is however necessary to determine reliable 3D models. In addition, the thermal aspects can not be neglected because they govern the shape memory effect. Indeed, thermal effects are preponderant during a dynamic adiabatic loading. In this paper, thermal and kinematic fields measurements are used to observe the austenite to martensite phase transformation in biaxial condition. Experiments are compared to the results of a finite difference axisymmetric model where the constitutive law is given by a fully coupled stochastic multi scale model. The first part is dedicated to the presentation of the experimental set-up and protocol, then experimental results are presented and compared to simulation, highlighting some dynamic effects not considered in the present modeling.

2 Experimental set-up

An home-made biaxial set-up coupled with a split Hopkinson system is used to submit the specimen to an equi-biaxial loading. Hopkinson systems allow high strain rates, about $10/s$ to $5000/s$ to be reached [3, 5]. The constitutive material of the bars is known and used in the field of linear elasticity, so that the system can be considered as a way of instrumentation. Strain gauges make it possible to determine the strain waves propagating in the bar and thus to evaluate forces and velocities conditions at the interfaces between bars and specimen. In the biaxial set-up (see figure 1), the impact is carried out by a single input bar, via a return angle system and two outgoing bars,

⋆ e-mail: quillery@lmt.ens-cachan.fr
⋆⋆ e-mail: durand@lmt.ens-cachan.fr
⋆⋆⋆ e-mail: hubert@lmt.ens-cachan.fr
⋆⋆⋆⋆ e-mail: zhao@lmt.ens-cachan.fr

so that the sample is loaded along two orthogonal directions. The angle deflection mechanism works thanks to two planes inclined at 45° relatively to the axis of the bar and allowing orthogonal compression.

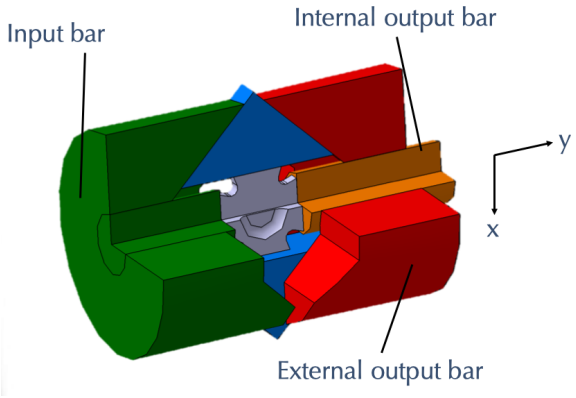

Figure 1: Set-up principle for dynamic equibiaxial compression test.

The Hopkinson formulae [3] firstly make it possible to determine the two orthogonal forces. We seek to determine the transition matrix from forces to stresses using equation (1), where m_{ij} parameters have to be identified using a finite element elastic modeling of the specimen structure.

$$\begin{pmatrix} \overline{\sigma_{xx}} \\ \overline{\sigma_{yy}} \end{pmatrix} = \begin{pmatrix} m_{xx} & m_{xy} \\ m_{yx} & m_{yy} \end{pmatrix} \begin{pmatrix} F_x \\ F_y \end{pmatrix} \quad (1)$$

Gauges are glued on incident and on the two transmitter bars to measure and calculate the strains thanks to usual Wheatstone bridge facilities (recording frequency is 500 KHz). The equibiaxial behavior is investigated in the study (angles of return angle system is fixed at 45°). The cruciform specimen is designed to concentrate stress in the central area (region of interest - ROI) and avoid buckling. The ROI is a 3 mm diameter circle with a thickness of 0.5 mm especially machined in the center of a 2 mm thick specimen. The maximum overall dimension is fixed by the Hopkinson bar system and the biaxial set-up. External dimension of specimen are 8 $mm \times 8\,mm$, the cruciform geometry is shown in figure (2a).

During the test, the biaxial specimen is tracked by a high speed numerical camera to accurately calculate its strain field by digital image correlation (DIC). The recording is realized by a SA5 fast-cam at 50000Hz and on a 512px × 271px area. The whole specimen surface is recorded to evaluate the free-body motions due to the Hopkinson bar system (kinematic boundary conditions). DIC principle consists to calculate the difference between two images, a reference one and a distorted one. An image is seen numerically as a function characterizing the gray level of each pixel. If we call $f(x)$ the function of the reference image and $g(x)$ the function of the deformed image, the determination of the displacement field $u(x)$ is obtained by minimizing equation (2).

$$g(x + u(x)) = f(x) \quad (2)$$

Correlation code (Correli-RT3) has been used considering the displacement field as continuous. This code allows the identification of displacement on each node of a finite element triangular mesh. The obtained displacement is regularized by an elastic solution [4]. A thermal camera placed in front of the other side of sample which has been painted in black allows the temperature field to be measured. A calibration of the infrared sensor with a black body allows the link between the digital level (function of electromagnetic radiation and emissivity) measured by the camera and the temperature to be obtained. Figure (2b) shows the full range calibration and the restricted area chosen to increase the recording frequency to 15000 Hz. This observation area, of about 64 × 8 pixels, enables to track the specimen during the testing and to compensate the free body displacement.

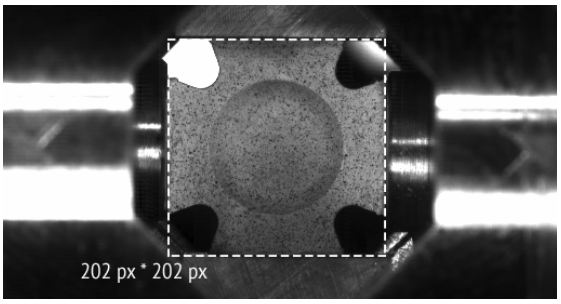

(a) Reference image and area for DIC

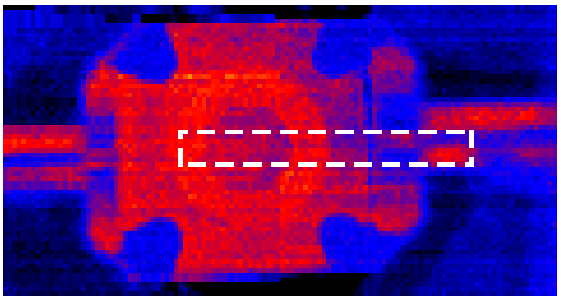

(b) Observation zone for a 15000 Hz infrared recording (64 $px \times 8\,px$)

Figure 2: Optical and thermal image settings

3 Experimental results

Figure 3a shows the strain measured by the gauges as function of time. After time shifting to virtually transport the signals from the strain gauges to the multi-axial set-up interfaces, and after Hopkinson formulae application, we can plot the forces and the velocities at these interfaces (figures 3b and 3c). During the steady state, all velocities are equal, and the forces applied by the incident and the transmitted bars are equal too. In our case, we have to compare the incident bar force to the sum of the two transmission bars forces to check at the equilibrium [6].

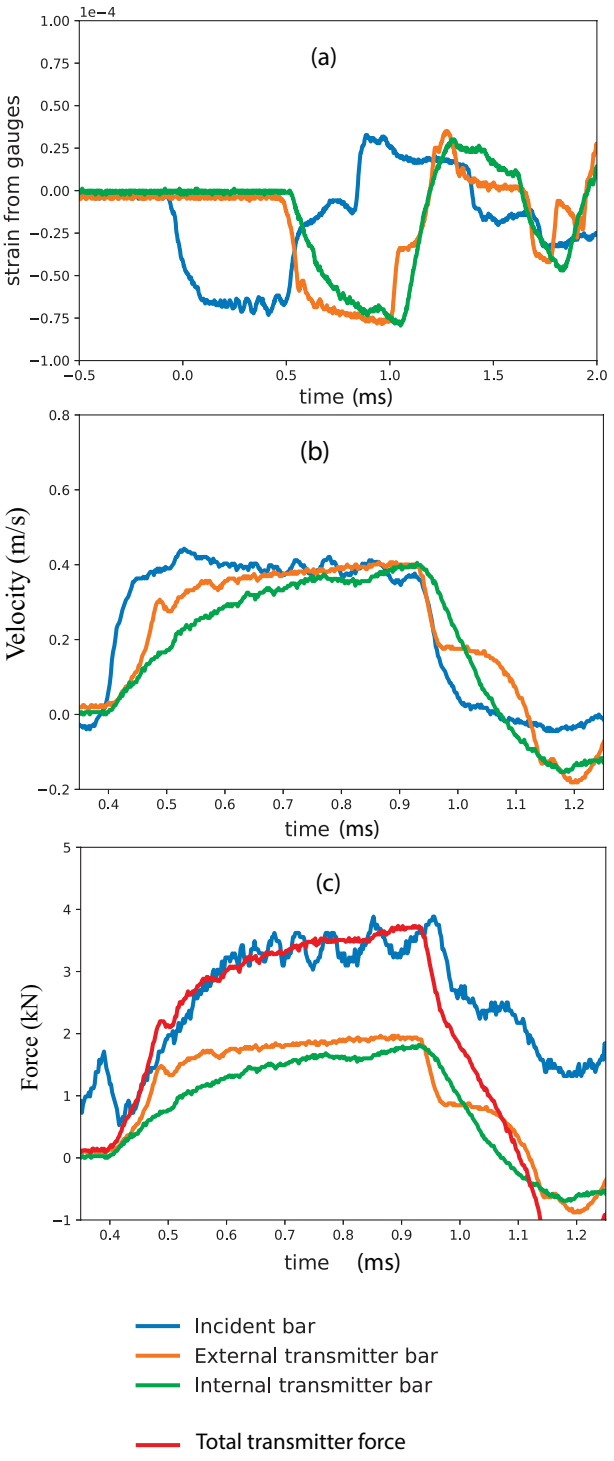

Figure 3: Measurements from bars: (a) strain from gauges, (b) velocities, and (c) forces in bars

These requirements are confirmed in figure 3c. However we observe that force in the internal transmitter bar is a few lower than the force in the external transmitter bar denoting that biaxial loading is not perfectly equiproportional. This difference can be explained by a friction in the biaxial set up, higher along x direction than along y direction. Average stress components σ_{xx} and σ_{yy} are calculated form forces thanks to equation 1 (parameters used are: $m_{xx} = m_{yy} = 0.2941\, mm^{-2}$ and $m_{xy} = m_{yx} = -0.0794\, mm^{-2}$). Strain components ϵ_{xx}, ϵ_{yy} and ϵ_{xy} are calculated in the ROI from DIC measurements. ϵ_{xx} and ϵ_{yy} are plotted as function of time in figure4a. Strains do not seem perfectly synchronized. The lower magnitude of ϵ_{yy} comparing to ϵ_{xx} is in accordance with the lower stress level along y axis. At the beginning, the strain along y can be related to a Poisson effect. At the end, the strain is reaching about 3.5%.

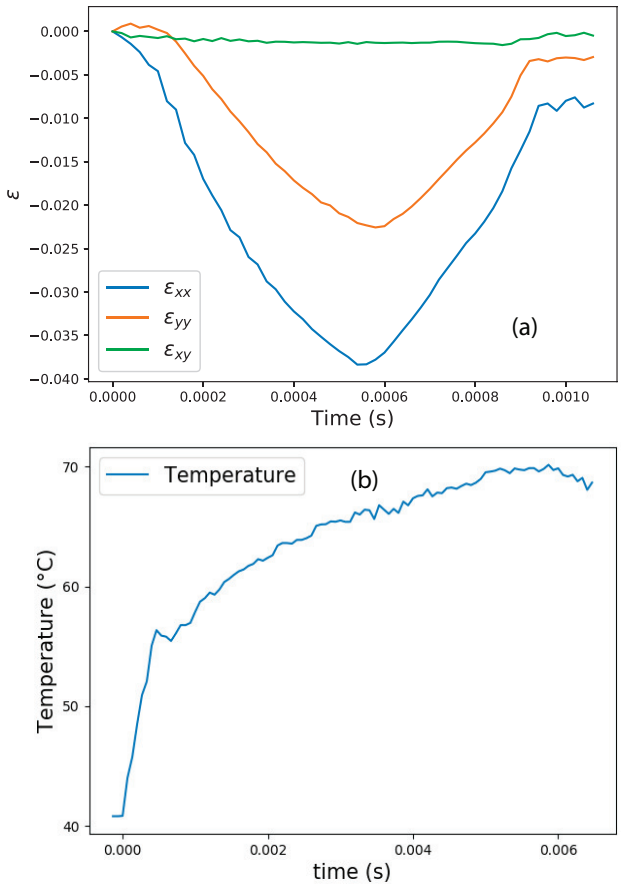

Figure 4: Average strain components and temperature over the ROI from DIC and infrared observations

Due to friction in the return angle system and micro clearance in the setup, the loading are not perfectly equibiaxial and perfectly reproducible. Figure 5 shows the stresses and strains multiaxial loading for two tests. For each case, the global loading is biaxial even if at the beginning, in the time to fill clearance it's look like unixial.

The infrared observations allow us to calculate the temperature increase during the test. Figure 6 illustrates this brutal increase during the first $1ms$. The evolution of average temperature with time in the ROI is reported in figure 4b showing that temperature is increasing from the very beginning of the test. However, it must be noticed that the temperature increases along a time range (about 6ms) much longer than the duration of mechanical loading (<1ms).

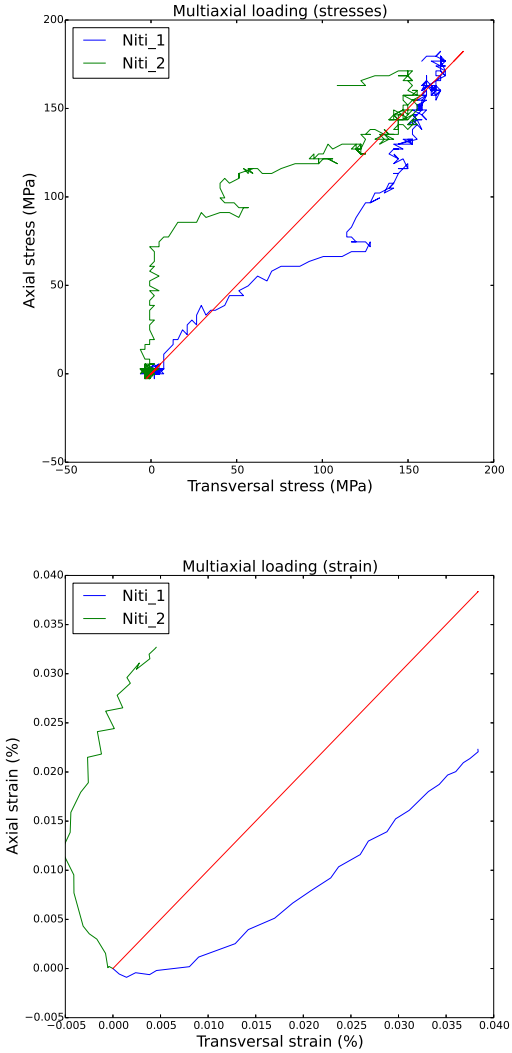

Figure 5: Multiaxial loading on two tests

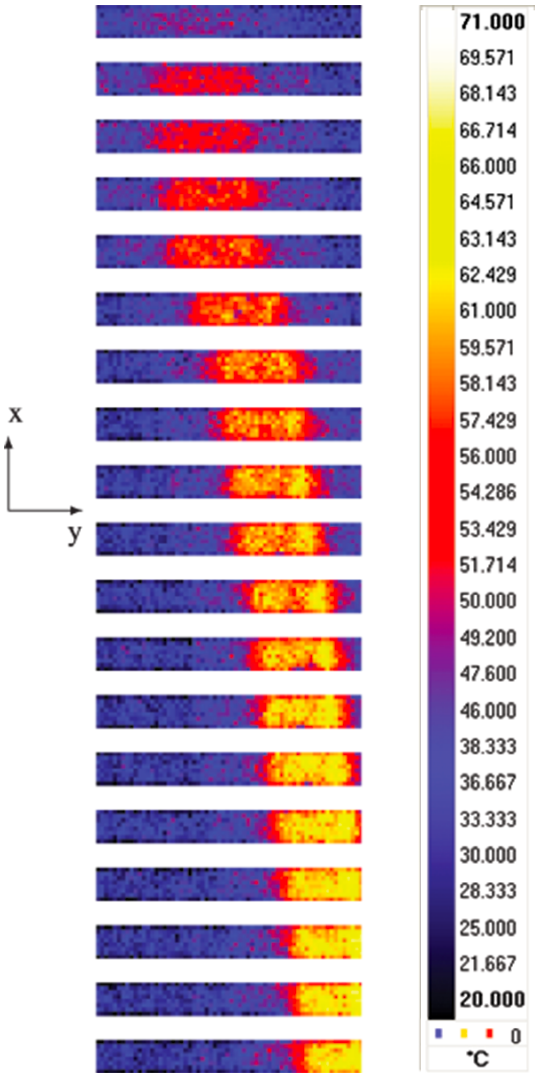

Figure 6: Sequence of frames from infrared camera (6ms).

4 Modeling

The numerical model used to describe the evolution of thermochemical fields is based on four scales: the variant scale α variant of a phase ϕ (martensite, R phase or austenite variants), the crystal g, the representative volume element (RVE) which is an assembly of crystals, and that of the structure. The single crystal model [7] predicts the distribution of the volume fractions f_{ϕ^α} of each variant in the grain from the calculation of their Gibbs free energy W_{ϕ^α} (3). The Gibbs free energy is the sum of chemical and elastic energies (4,5), calculated from the knowledge of the enthalpies and entropies of each phase (h_ϕ, s_ϕ), of the transformation strain (Green-Lagrange tensor) of each of variants $\boldsymbol{\epsilon}^{tr}_{\phi^\alpha}$ (12 variants of monoclinic martensite, 4 variants of rhombohedral R phase and 1 variant of cubic austenite), of the stiffness tensor of the medium $\mathbb{C}_\phi$, the temperature T_{ϕ^α} and the stress $\boldsymbol{\sigma}_{\phi^\alpha}$ (considered as homogeneous in the RVE to fasten the calculations). The fraction of each phase is estimated via a Boltzmann probability distribution (6), often used in magneto-mechanical problems [8], where A_s is a parameter identified from a calorimetry measurement.

$$W_{\phi^\alpha} = W^T_{\phi^\alpha} + W^\sigma_{\phi^\alpha} \tag{3}$$

$$W^T_{\phi^\alpha} = h_\phi - T_{\phi^\alpha} s_\phi \tag{4}$$

$$W^\sigma_{\phi^\alpha} = -\frac{1}{2}\boldsymbol{\sigma}_{\phi^\alpha} : \mathbb{C}^{-1}_\phi : \boldsymbol{\sigma}_{\phi^\alpha} - \boldsymbol{\sigma}_{\phi^\alpha} : \boldsymbol{\epsilon}^{tr}_{\phi^\alpha} \tag{5}$$

$$f_{\phi^\alpha} = \frac{exp(-A_s W_{\phi^\alpha})}{\sum_{\phi=1}^{n}\sum_{\alpha=1}^{m} exp(-A_s W_{\phi^\alpha})} \tag{6}$$

The modeling of the polycrystal behavior is based on the scaling up by simple averaging of the quantities by crystal (using localization procedures if need be). For this, the RVE is described as an aggregate of single crystals via an Orientation Distribution Function (ODF). The RVE is composed of about 100 orientations for the calculation. The physical parameters used for the modeling are gathered in 1. A Backward Euler Finite Difference decomposition of the sample has been done in axisymmetic condition using Neumann Boundary condition (adiabatic condition), where phase fraction ratio acts as heat sources in the heat equation (7) [1].

$$\rho C_p \frac{dT}{dt} = k\frac{d^2T}{dr^2} + \frac{k}{r}\frac{dT}{dr} - (h_M - h_R)\frac{df_M}{dt} + (h_R - h_A)\frac{df_A}{dt} \quad (7)$$

Using the numerical discretization :

$$\frac{dT}{dt} = \frac{T_j^{n+1} - T_j^n}{\Delta t} \quad (8)$$

$$\frac{df_M}{dt} = \frac{{f_M}_j^{n+1} - {f_M}_j^n}{\Delta t} \quad \text{and} \quad \frac{df_A}{dt} = \frac{{f_A}_j^{n+1} - {f_A}_j^n}{\Delta t} \quad (9)$$

$$\frac{d^2T}{dr^2} = \frac{T_{j+1}^{n+1} - 2T_j^{n+1} + T_{j-1}^{n+1}}{\Delta r^2} \quad (10)$$

$$\frac{dT}{dr} = \frac{T_{j+1}^{n+1} - T_j^{n+1}}{\Delta r^2} \quad (11)$$

A scalar representation of experimental and modeled stress-strain behaviors has been plotted in figure 7a (using a von Mises and Levy-Mises standardization for stress and strain. eq.(12) and (13)). We observe first in figure 6a that the threshold from elastic to inelastic transition (phase transition characterized by a plateau) seems underestimated by the modeling. This difference may be explained by the existence of some micro-inertia phenomena associated with the phase transition (rotation of crystallographic lattice) and ignored by the modeling. This underestimation happens although the temperature increase is overestimated at the very beginning of the loading (figure 6b). Indeed, the experimental temperature emission is spread over a much longer duration than the emission duration provided by the model, in direct relation with the duration of the shock. This difference may be explained by the existence of incubation delay associated with the germination of martensite in austenite. This phenomenon is ignored by the modeling. Despite this discrepancy, experimental and modeled final temperatures are in accordance, validating the adiabatic thermal boundary conditions.

$$\sigma_{VM} = \sqrt{\frac{1}{2}\left(\left(\sigma_{xx} - \sigma_{yy}\right)^2 + \sigma_{xx}^2 + \sigma_{yy}^2\right)} \quad (12)$$

$$\epsilon_{LV} = \sqrt{\frac{2}{3}\left(\epsilon_{xx}^2 + \epsilon_{yy}^2 + 2\epsilon_{xy}^2\right)} \quad (13)$$

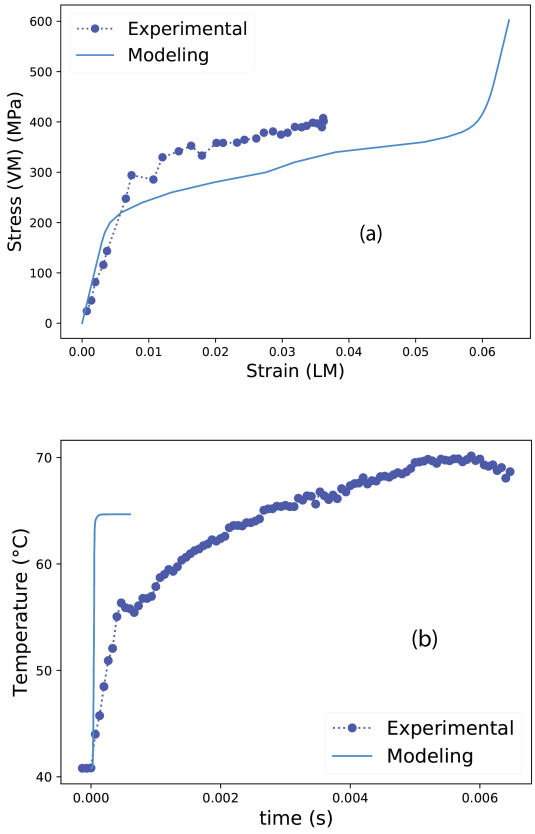

Figure 7: Comparison experiments modeling: (a) Normalized stress-strain behavior; (b) Temperature release.

	h_ϕ (MJ/m^3)	s_ϕ (273K) (MJ/m^3)	lattice parameters (nm)
A	-110	0.72	a=b=c=0.3017
R	-254	0.57	a=b=0.734 c=0.527
M	-293	0.20	a=0.290 b=0.411 c=0.465

	lattice angles (°)	C_{ij} (Voigt) (GPa)
A	α=β=γ=90	
R	α=γ=90, β=120	C_{11}=238, C_{12}=142, C_{44}=232
M	α=γ=90, β=97.8	

ρ (kg/m^3)	C_p (J/kg/K)	A_s (m^3/J)
6450	900	2.54e-06

Table 1: Physical constants used for the multiscale modeling

5 Conclusion

In this study, the multi-axial dynamic behavior of a NiTi alloy has been prospected and compared to the results of axisymmetric finite difference modeling including a multiscale and multiphysic constitutive law. Despite very strong assumption considering the mechanical and thermal boundary conditions, interesting qualitative results have been obtained. Improvements may be achieved by more

representative boundary conditions, the introduction of micro- inertial phenomena in the modeling, and a time delay in martensite production able to model the heat emission more accurately.

References

[1] D. Depriester, A. Maynadier, K. Lavernhe-Taillard, O. Hubert, "Thermomechanical modelling of a NiTi SMA sample submitted to displacement-controlled tensile test" **International Journal of Solids and Structures**, *51*, 10 (2014) 1901-1922.

[2] R. Adharapurapu, F. Jiang, S.Vecchio and G. T. Gray, Response of NiTi shape memory alloy at high strain rate: A systematic investigation of temperature effects on tension–compression asymmetry **Acta Materialia**, (2006)

[3] B. Hopkinson. A method of measuring the pressure produced in the detonation of high explosives or by the impact of bullets, **Philosophical Transactions of the Royal Society of London**, 213 :437–456 (1914)

[4] Z. Tomicevc, F. Hild, S. Roux. Mechanics-aided digital 492 image correlation. **Journal of Strain Analysis**, 48(5)

[5] E.Davies and S. Hunter. The dynamic com- pression testing of solids by the method of the split hopkinson pressure bar. **Journal of the Mechanics and Physics of Solids**. (1963)

[6] H.Zhao and G.Gary. On the use of SHPB technique to determine the dynamic behavior of the materials in the range of small strains. **International Journal of Solids and structures**, (1996)

[7] A. Maynadier, D. Depriester, K. Lavernhe-Taillard and O.Hubert, "Thermo-mechanical description of phase transformation in Ni-Ti Shape Memory Alloy", **Procedia Engineering**, *10* (2011) 2214-2219.

[8] X. Wang, O. Hubert, S. He, F.S. Mballa-Mballa, Y. Huang, "Reversible magneto-mechanical modeling of heterogeneous media", **Journal of Superconductivity and Novel Magnetism**, *27*, 9 (2014) 2049-2058.